



**HAL**  
open science

# Ultrabroadband Optical Phenomena in Quadratic Nonlinear Media

Matteo Conforti, F. Baronio, C de Angelis

► **To cite this version:**

Matteo Conforti, F. Baronio, C de Angelis. Ultrabroadband Optical Phenomena in Quadratic Nonlinear Media. *IEEE Photonics Journal*, 2010, 2 (4), pp.600-610. 10.1109/JPHOT.2010.2051537. hal-02395464

**HAL Id: hal-02395464**

**<https://hal.science/hal-02395464v1>**

Submitted on 5 Dec 2019

**HAL** is a multi-disciplinary open access archive for the deposit and dissemination of scientific research documents, whether they are published or not. The documents may come from teaching and research institutions in France or abroad, or from public or private research centers.

L'archive ouverte pluridisciplinaire **HAL**, est destinée au dépôt et à la diffusion de documents scientifiques de niveau recherche, publiés ou non, émanant des établissements d'enseignement et de recherche français ou étrangers, des laboratoires publics ou privés.

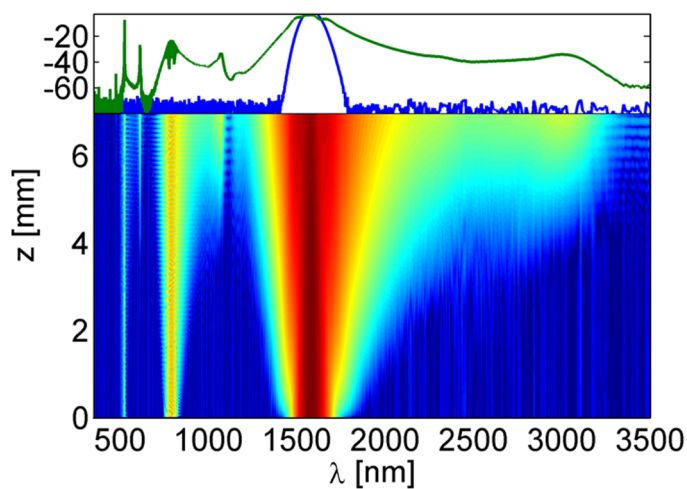
# Ultrabroadband Optical Phenomena in Quadratic Nonlinear Media

Volume 2, Number 4, August 2010

M. Conforti

F. Baronio, Member, IEEE

C. De Angelis, Member, IEEE



DOI: 10.1109/JPHOT.2010.2051537

1943-0655/\$26.00 ©2010 IEEE

# Ultrabroadband Optical Phenomena in Quadratic Nonlinear Media

M. Conforti, F. Baronio, *Member, IEEE*, and C. De Angelis, *Member, IEEE*

CNISM, Dipartimento di Ingegneria dell'Informazione, Università di Brescia, 25123 Brescia, Italy

DOI: 10.1109/JPHOT.2010.2051537  
1943-0655/\$26.00 ©2010 IEEE

Manuscript received April 22, 2010; revised May 24, 2010; accepted May 24, 2010. Date of publication May 26, 2010; date of current version June 22, 2010. Corresponding author: M. Conforti (e-mail: matteo.conforti@ing.unibs.it).

**Abstract:** We present a comprehensive framework to study the nonlinear evolution of ultrabroadband optical pulses in quadratic nonlinear media. We employ a nonlinear envelope equation that goes beyond the traditional slowly varying approximation and allows treatment of all the harmonics by means of a single equation. We exploit this model to simulate recently observed supercontinuum phenomena such as ultrabroadband parametric downconversion and the generation of octave-spanning spectra from femtosecond pulses.

**Index Terms:** Supercontinuum generation, nonlinear crystals, second-harmonic generation.

## 1. Introduction

Spectral broadening and the generation of new frequency components are the characterizing features of nonlinear optics and have been studied intensively since the early 1960s. There is a family of processes known as supercontinuum generation [1] that occurs when narrow-band incident pulses undergo extreme nonlinear spectral broadening to yield a broadband spectrally continuous output. Supercontinuum generation was first reported in the 1970s and, since then, has been the subject of numerous investigations in a wide variety of nonlinear media.

The overwhelming majority of studies on supercontinuum generation deal with third-order nonlinear media, characterized by Kerr and Raman processes. This fact is mainly due to the advent of a new class of optical waveguides: The photonic crystal fiber (PCF), in the late 1990s, attracted widespread interest throughout the scientific community and has led to a revolution in the generation of ultrabroadband high brightness spectra through supercontinuum generation. This fact has also attracted theoretical research efforts on the modeling of broadband phenomena that take place in cubic media. Different models that allow the description of supercontinuum generation in cubic media were proposed in the literature, the most well-known being the generalized nonlinear Schrödinger equation (GNLS) [2].

There are a few experimental works that report the observation of extremely broad spectrum generation by exploiting second-order nonlinear materials such as Lithium Niobate (LN), Lithium Tantalate (LT), and Potassium Dihydrogen Phosphate (KDP) or Potassium Titanium Oxide Phosphate (KTP) [3]–[7]. In the framework of quadratically nonlinear media, a quasi-phase matching technique can be used to engineer nonlinear structures [8]. This technique opens a whole range of new possibilities and shows great promise for use in entangled photon (biphoton) generation [9], [10], quantum optical coherence tomography [11], and Coherent Anti-Stokes Raman Spectroscopy (CARS) [12]. Theoretical research efforts on the modeling of this kind of broadband phenomenon are more limited.

From the theoretical side, the analysis of optical pulse propagation typically involves the definition of a complex envelope whose variation is supposed to be “slow” with respect to the oscillation of a

carrier frequency (slowly varying envelope approximation (SVEA) [2]). In the frequency domain, this assumption is equivalent to requiring that the bandwidth of the envelope is narrow with respect to the carrier frequency. Different works showed that it is possible to extend the validity of a proper generalization of the envelope equation to pulse duration down to the single optical oscillation cycle and to the generation of very broad spectra [13]–[23].

When second-order nonlinearities are considered, the usual approach is to write coupled equations for the separated frequency bands relevant for the process [20]. However, when ultrabroadband  $\chi^{(2)}$  phenomena take place, the fundamental frequency and harmonics bands merge, generating a single broad spectrum, as observed in recent experiments [3]. Obviously, in these cases, the coupled envelope description of the propagation fails due the frequency overlapping of the distinct bands.

The scope of this article is to exploit a recently derived [24] single-wave envelope equation for the description of ultrabroadband  $\chi^{(2)}$  interactions. This model, besides providing a powerful tool for analytical treatment due to its simplicity, can be easily solved with a modest computational effort and can be easily generalized by including other kinds of nonlinearities.

We recall the derivation of the master equation in Section 2, discussing the approximations and the limit of validity of the model. In Section 3, we analyze some experimental results of broadband generation in quadratic media, finding an excellent agreement between the measured data and the numerics. Finally, we present our conclusions in Section 4.

## 2. Derivation of the Master Equation

### 2.1. Unidirectional Field Equation

Our derivation of the envelope equation, for that which concerns the linear dispersive terms, builds upon the work of Brabec and Krausz [13], who carried a simple model that was shown (theoretically and experimentally) to be accurate in most situations. Starting from Maxwell equations (written in MKS units), neglecting transverse dimensions (i.e., considering the propagation of plane waves), we can obtain the 1 + 1D wave equation for the electric field  $E(z, t)$

$$\frac{\partial^2 E(z, t)}{\partial z^2} - \frac{1}{c^2} \frac{\partial^2}{\partial t^2} \int_{-\infty}^{+\infty} E(z, t') \varepsilon(t - t') dt' = \frac{1}{\varepsilon_0 c^2} \frac{\partial^2}{\partial t^2} P_{NL}(z, t). \quad (1)$$

The choice of neglecting transverse spatial dimensions is not a loss of generality in our model, because, in the physical set-ups we want to describe, they can be factored out and treated as a different problem.

By defining the Fourier transform  $\mathcal{F}[E](\omega) = \hat{E}(\omega) = \int_{-\infty}^{+\infty} E(t) e^{-i\omega t} dt$ , we can write (1) in frequency domain:

$$\frac{\partial^2 \hat{E}(z, \omega)}{\partial z^2} + \frac{\omega^2}{c^2} \hat{\varepsilon}(\omega) \hat{E}(z, \omega) = -\frac{\omega^2}{\varepsilon_0 c^2} \hat{P}_{NL}(z, \omega) \quad (2)$$

where  $c$  is the vacuum velocity of light,  $\varepsilon_0$  is the vacuum dielectric permittivity,  $\hat{\varepsilon}(\omega) = 1 + \hat{\chi}(\omega)$ ,  $\hat{\chi}(\omega)$  is the linear electric susceptibility, and  $k(\omega) = (\omega/c) \sqrt{\hat{\varepsilon}(\omega)}$  is the propagation constant.

We now factor out the fast dependence of the propagation coordinate from the electric field for all the frequencies:  $\hat{E}(z, \omega) = \hat{U}(z, \omega) \exp[-ik(\omega)z]$ . This definition amounts to writing the electric field as the product of a spatial carrier wave and a slowly varying envelope. Since we remove the exact propagation constant at every frequency, we can avoid making a requirement on the bandwidth of the pulses. Wave equation for the field  $\hat{U}$  reads

$$\frac{\partial^2 \hat{U}(z, \omega)}{\partial z^2} - 2ik(\omega) \frac{\partial \hat{U}(z, \omega)}{\partial z} = -\frac{\omega^2}{\varepsilon_0 c^2} \hat{P}_{NL}(z, \omega) e^{ik(\omega)z}. \quad (3)$$

We make the slowly evolving wave approximation (SEWA), that is  $|\partial_z \hat{U}| \ll 2k(\omega)|\hat{U}|$ , and thus, we can write

$$\frac{\partial \hat{U}(z, \omega)}{\partial z} = -i \frac{\omega^2}{2\varepsilon_0 c^2 k(\omega)} \hat{P}_{NL}(z, \omega) e^{ik(\omega)z} \quad (4)$$

and from the definition of  $\hat{U}$ , we obtain the equation for the electric field:

$$\frac{\partial \hat{E}(z, \omega)}{\partial z} + ik(\omega)\hat{E}(z, \omega) = -i \frac{\omega}{2\varepsilon_0 c n(\omega)} \hat{P}_{NL}(z, \omega). \quad (5)$$

This equation has been found by a heuristic method and has been termed the Forward Maxwell Equation (FME) [16]. Once the form of nonlinearity is specified, for example, a second-order instantaneous nonlinear polarization  $\hat{P}_{NL}(z, \omega) = \varepsilon_0 \chi^{(2)} \mathcal{F}[E(z, t)^2](\omega)$ , we can directly solve (5) in the frequency domain with a standard split-step Fourier method. When backward waves can be neglected, this equation is equivalent to Maxwell equations [16], [22], but the numerical solution is much more efficient. However, we can further simplify (5) by opportunely defining an envelope.

## 2.2. Definition of the Envelope

We consider the electric field  $E$  and the nonlinear polarization  $P_{NL}$  as the product of a complex envelope and a carrier wave

$$E(z, t) = \frac{1}{2} A(z, t) e^{i\omega_0 t - i\beta_0 z} + c.c. \quad (6)$$

$$P_{NL}(z, t) = \frac{1}{2} A_p(z, t) e^{i\omega_0 t - i\beta_0 z} + c.c. \quad (7)$$

that, in the frequency domain, reads

$$\begin{aligned} \hat{E}(z, \omega) &= \frac{1}{2} \hat{A}(z, \omega - \omega_0) e^{-i\beta_0 z} + \frac{1}{2} \hat{A}^*(z, -\omega - \omega_0) e^{i\beta_0 z} \\ \hat{P}_{NL}(z, \omega) &= \frac{1}{2} \hat{A}_p(z, \omega - \omega_0) e^{-i\beta_0 z} + \frac{1}{2} \hat{A}_p^*(z, -\omega - \omega_0) e^{i\beta_0 z} \end{aligned}$$

where  $\omega_0$  is a reference frequency,  $\beta_0 = \text{Re}[k(\omega_0)]$ , and  $k(\omega) = (\omega/c) \sqrt{\hat{\varepsilon}(\omega)}$  is the propagation constant.

Particular care must be devoted to the definition of the complex envelope, since we do not want to put any limitations on the frequency extent of the signals. This aspect is commonly overlooked in the literature, and it is taken for granted that the band of the envelope is ‘‘narrow’’ in some sense. We shall see later that for quadratically nonlinear media, a proper definition of the envelope is crucial. As usual, in the theory of modulation [25], we define the analytic representation of the electric field

$$\tilde{E}(z, t) = E(z, t) + i\mathcal{H}[E](z, t) \quad (8)$$

where

$$\mathcal{H}[E](z, t) = \frac{1}{\pi} p.v. \int_{-\infty}^{+\infty} \frac{E(z, t')}{t - t'} dt' \quad (9)$$

is the Hilbert transform of the electric field (*p.v.* indicates the Cauchy principal value of the integral). The Fourier transform of the analytic signal reads

$$\hat{\tilde{E}}(z, \omega) = \begin{cases} 2\hat{E}(z, \omega), & \text{if } \omega > 0 \\ \hat{E}(z, 0), & \text{if } \omega = 0 \\ 0, & \text{if } \omega < 0 \end{cases} \quad (10)$$

that is a signal that contains only the positive frequency content of the electric field. Due to the reality of  $E(z, t)$ , its Fourier transform has Hermitian symmetry so that only the positive (or the negative) frequencies carry information, and we can write

$$\hat{E}(z, \omega) = \frac{1}{2} \hat{E}(z, \omega) + \frac{1}{2} \hat{E}^*(z, -\omega) \quad (11)$$

and eventually, we can define the complex electric field envelope as

$$A(z, t) = \tilde{E}(z, t) e^{-i\omega_0 t + i\beta_0 z} \quad (12)$$

i.e., the inverse Fourier transform of the positive frequency content of  $E$  shifted toward the low frequency part of the spectrum by an amount  $\omega_0$ . *It is worth noting that no approximations on the frequency extent of the envelope has been done; therefore,  $\text{supp}\{\hat{A}(z, \omega)\} = (-\omega_0, +\infty)$ .*

### 2.3. Nonlinear Envelope Equation

The substitution of expressions of  $\hat{E}(z, \omega)$  and  $\hat{P}_{NL}(z, \omega)$  in (5) and the Taylor-expansion of  $k(\omega)$  about  $\omega_0$  yields

$$\frac{\partial \hat{A}(z, \Omega)}{\partial z} + i \left[ \sum_{m=1}^{\infty} \frac{k_m}{m!} \Omega^m \right] \hat{A}(z, \Omega) = -i \frac{\omega}{2n(\omega)c\epsilon_0} \hat{A}_p(z, \Omega) \quad (13)$$

where  $\Omega = \omega - \omega_0$ , and  $k_m = (\partial^m k / \partial \omega^m)(\omega_0)$ .

In order to obtain a time domain equation, we have to perform another approximation, i.e., on the right-hand side of (13), we have to impose  $n(\omega)$  nearly constant in the band of interest. Since we want to take into account ultrabroad spectra, we require the validity on band whose order of magnitude is the same of the carrier frequency, that is  $(\partial n(\omega) / \partial \omega)|_{\omega_0} \omega_0 \ll n(\omega_0)$  (this is equivalent to the requirement  $|(\beta_0 - \omega_0 k_1) / \beta_0| \ll 1$  used in [13]). Far from resonances, this requirement is fulfilled in the majority of parametric processes in which all waves propagate in the same direction.

By inverse Fourier transform, we obtain from (13)

$$\frac{\partial A(z, t)}{\partial z} + iD'A(z, t) = -i \frac{\omega_0}{2n_0 c \epsilon_0} \left( 1 - \frac{i}{\omega_0} \frac{\partial}{\partial t} \right) A_p(z, t) \quad (14)$$

where we have defined the dispersive operator  $D' = \sum_{m=1}^{\infty} (1/m!) k_m (-i(\partial/\partial t))^m$ . As a last step, we rewrite (14) in a reference frame moving at the group velocity at reference frequency by the change of variables  $z' = z$  and  $\tau = t - k_1 z$ , thus obtaining

$$\frac{\partial A(z', \tau)}{\partial z'} + iDA(z', \tau) = -i \frac{\omega_0}{2n_0 c \epsilon_0} \left( 1 - \frac{i}{\omega_0} \frac{\partial}{\partial \tau} \right) A_p(z', \tau) \quad (15)$$

where  $D = \sum_{m=2}^{\infty} (1/m!) k_m (-i(\partial/\partial \tau))^m$ .

We note that the derivation outlined here makes less-stringent assumptions than the original derivation proposed by Brabec and Krausz. In fact, we performed the slowly evolving approximation directly on the wave equation for the field  $E$  and not for the envelope  $A$ . In this way, the choice of the reference frequency  $\omega_0$  and the change of reference frame is done only for convenience and is not essential to obtain the equation. In contrast, they are key points in the classical derivation of the NEE [13], as reviewed also in [2]. The differences between the two procedures can be ascribed to the fact that the derivation of Brabec and Krausz is essentially performed in time domain, and it is equivalent in our case to making the definition of the ‘‘pre-envelope’’  $\hat{E}(z, \omega) = \hat{U}(z, \omega) \exp[-ik(\omega)z] \approx \hat{U}(z, \omega) \exp[-i(k_0 + k_1(\omega - \omega_0))z]$ .

### 2.4. Nonlinear $\chi^{(2)}$ Polarization

We now consider an instantaneous second-order  $\chi^{(2)}$  nonlinearity, giving rise to the following nonlinear polarization:

$$\begin{aligned} P_{NL}(z, t) &= \varepsilon_0 \chi^{(2)} E(z, t)^2 \\ &= \varepsilon_0 \chi^{(2)} \operatorname{Re}[A(z, t) e^{i\omega_0 t - i\beta_0 z}]^2 \\ &= \frac{\varepsilon_0 \chi^{(2)}}{4} \left[ A^2 e^{2i\omega_0 t - 2i\beta_0 z} + A^{*2} e^{-2i\omega_0 t + 2i\beta_0 z} + 2|A|^2 \right]. \end{aligned} \quad (16)$$

It is worth noting that, due to the definition of  $A$ , the first (second) term in the square brackets contains only positive (negative) frequencies, whereas the third has both. It is now apparent that it is impossible to separate the nonlinear polarization in two distinct and “narrow” bands for the positive and negative frequencies, which is common in cubic media. Moreover, neglecting of the third term leads to totally wrong results (this term is responsible for difference frequency generation). By going through steps (8)–(12), we can instead correctly define the nonlinear polarization envelope

$$A_p(z, t) = \tilde{P}_{NL}(z, t) e^{-i\omega_0 t + i\beta_0 z} = \frac{\varepsilon_0 \chi^{(2)}}{2} \left[ A^2 e^{i\omega_0 t - i\beta_0 z} + \left( |A|^2 + i\mathcal{H}[|A|^2] \right) e^{-i\omega_0 t + i\beta_0 z} \right]. \quad (17)$$

Before inserting (17) into (15), the term  $|A|^2$  in (16) and (17) deserves further comment since it is centered around zero in frequency domain. In particular, to obtain the nonlinear polarization envelope in (17), we had to filter out the negative frequency components of  $\hat{P}_{NL}(\omega)$ , as was done for  $\hat{E}(\omega)$ . We note, however, that (i)  $\hat{A}(z, \omega - \omega_0)$  does not contain negative frequency by definition, (ii)  $P_{NL}$  is a small perturbation to linear polarization, and (iii) negative frequencies cannot be phase-matched. It follows that the task of filtering the negative frequency components of  $|A|^2$  can be left to the propagation equation instead of having it explicitly in the definition of  $A_p(z, t)$ . In other words, when inserting (17) into (15), we can write  $|A|^2 + i\mathcal{H}[|A|^2] \approx 2|A|^2$ . We have checked numerically the good accuracy of this approximation. Even if this approximation is not necessary in the numerical solution (it is straightforward to calculate the exact nonlinear polarization envelope in frequency domain), it is suitable to obtain a simple and manageable model for further analytical investigations.

The NEE for  $A = A(z', \tau)$  becomes

$$\frac{\partial A}{\partial z'} + iDA = -i \frac{\chi^{(2)} \omega_0^2}{4\beta_0 c^2} \left( 1 - \frac{i}{\omega_0} \frac{\partial}{\partial \tau} \right) \left[ A^2 e^{i\omega_0 \tau - i(\beta_0 - k_1 \omega_0) z'} + 2|A|^2 e^{-i\omega_0 \tau + i(\beta_0 - k_1 \omega_0) z'} \right] \quad (18)$$

or, performing derivatives

$$\frac{\partial A}{\partial z'} + iDA = -i \frac{\chi^{(2)} \omega_0^2}{4\beta_0 c^2} \left[ \left( 2A^2 - \frac{2i}{\omega_0} A \frac{\partial A}{\partial \tau} \right) e^{i\omega_0 \tau - i(\beta_0 - k_1 \omega_0) z'} - \frac{4i}{\omega_0} \operatorname{Re} \left[ A^* \frac{\partial A}{\partial \tau} \right] e^{-i\omega_0 \tau + i(\beta_0 - k_1 \omega_0) z'} \right]. \quad (19)$$

These first-order nonlinear envelope equations in the propagation coordinate provide a powerful means of describing light pulse propagation in dispersive quadratically nonlinear media.

Starting from (18), it is straightforward to show that our equation conserves the total energy of the field, i.e.,  $(d/dz') \int_{-\infty}^{+\infty} |A(z', \tau)|^2 d\tau = 0$ . It can also be shown that the total energy is conserved even if the nonapproximated nonlinear polarization envelope  $A_p$  [see (17)] is used (see the Appendix).

## 3. Numerical Results

The forward Maxwell equation (5) and nonlinear envelope equation (18) can be solved easily by the split-step Fourier method exploiting the fourth-order Runge–Kutta scheme for the nonlinear step. In this Section, we show a few examples of full numerical modeling of the experimentally measured broadband output spectra.

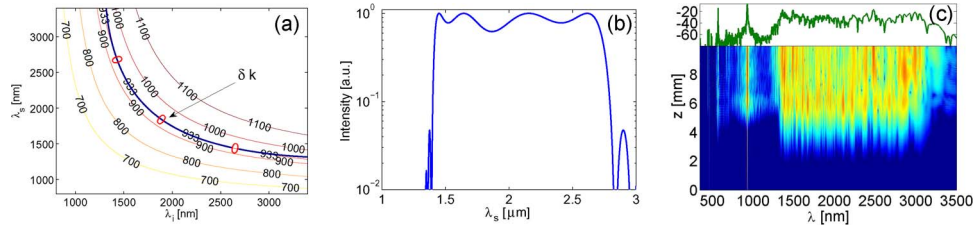


Fig. 1. (a) Level curves of pump wavelength and of mismatch  $\delta k = 0$  in the  $\lambda_i - \lambda_s$  plane. (b) OPG gain bandwidth in the limit of small gain [2] for a 10-mm-long PPLN. QPM period  $\Lambda = 27 \mu\text{m}$  and temperature  $T = 24 \text{ }^\circ\text{C}$ . (c) Evolution of the power spectrum (in decibels) from the numerical solution of (18) and power spectrum profile at the crystal output. The initial pulse has Gaussian shape, and the parameters are  $T = 1 \text{ ps}$ ,  $I = 2 \text{ GW/cm}^2$ ,  $\lambda_p = 933 \text{ nm}$ ,  $\lambda_0 = 2\pi c/\omega_0 = 700 \text{ nm}$ , and  $d_{33} = \chi_{LN}^{(2)}/2 = 27 \text{ pm/V}$ .

### 3.1. Broadband Parametric Generation

As a first example, we consider the collinear broadband optical parametric generation (OPG) using periodically poled crystals [4], [5]. In this process, an intense narrow-band laser beam called the pump is down-converted to two lower frequency beams, called the signal and the idler, satisfying  $\omega_p = \omega_s + \omega_i$  and having wave vector mismatch  $\Delta k = k_p - k_s - k_i$ . Thanks to the periodic poling, the residual mismatch  $\delta k = \Delta k - 2\pi/\Lambda$  can be eliminated at some frequencies. Broadband OPG is accomplished by choosing a specific combination of poling period and pump wavelength that allows the group velocity of the signal and the idler to closely match at the degeneracy point.

We considered an LN sample, and to model the refractive index dispersion, we employed a Sellmeier model fitted from experimental data [26]. In this case, the optimal poling period and pump wavelength combination was found to be  $\Lambda = 27 \mu\text{m}$  and  $\lambda_p = 933 \text{ nm}$  [4]. Fig. 1(a) shows the pump wavelength and the mismatch curve  $\delta k = 0$  as functions of  $\lambda_{i,s}$  for a fixed poling period  $\Lambda = 27 \mu\text{m}$  and a temperature  $T = 24 \text{ }^\circ\text{C}$ . It can be seen that the mismatch curve and the  $\lambda_p = 933 \text{ nm}$  curve are practically superimposed in a wavelength range 1500 nm–3000 nm. This superposition suggests that in this range, the parametric gain will be high, as confirmed by Fig. 1(b).

We simulated the propagation of a  $T = 1 \text{ ps}$  FWHM long Gaussian pulse, centered around 933 nm, with  $I = 2 \text{ GW/cm}^2$  peak intensity. In the simulation, we set the reference wavelength  $\lambda_0 = 700 \text{ nm}$  in order to minimize the width of the numerical temporal window. We assumed a nonlinear coefficient  $d_{33} = \chi_{LN}^{(2)}/2 = 27 \text{ pm/V}$  and modeled the square-wave QPM grating as a sum of spatial harmonics up to the fifth order. In the numerical code, we inserted the exact dispersion relation  $k(\omega)$  as obtained from the Sellmeier relation.

Fig. 1(c) shows the evolution of the power spectrum obtained from numerical solution of (18). The input narrow-band pump, due to the presence of noise, is down-converted to the phase-matched signal and idler that are located in the 1500 nm–3500 nm region. This region is slightly larger than the one predicted by small gain approximation, since the high intensity leads to a parametric gain broadening [27]. After the down-converted continuum is generated, say after  $z = 4 \text{ mm}$ , it interacts with the pump through cascading processes that leads to a spectral broadening of the depleted pump. Moreover, an intense peak in the visible range at  $\lambda_3 = 575 \text{ nm}$  appears, due to the sum frequency generation of the pump and the generated component at  $\lambda = 1500 \text{ nm}$ , matched through the third spatial harmonic of the grating. These numerical results compare well with experiments reported in [4].

It is worth noting that such a broad spectrum can by no means be studied with standard coupled-wave models. In fact, the spectral extent of the signal and idler signals is more than an octave, and they overlap in the spectral domain.

### 3.2. Parametric Generation in Chirped Structure

In the previous example, we showed that the frequency range of the generated broadband continuum is fixed by the dispersive properties of the material. A way to engineer the parametric



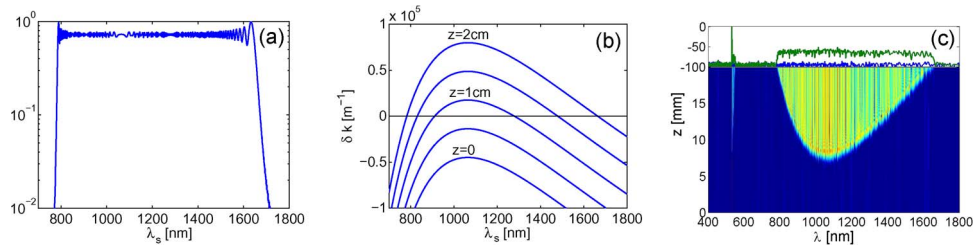


Fig. 2. (a) OPG gain bandwidth in the limit of small gain for a 20-mm-long PPSLT for the chirped QPM grating; temperature  $T = 80$  °C. (b) Local phase-matching curves as a function of propagation distance. (c) Evolution of the power spectrum (in decibels) from numerical solution of (18) and power spectrum profile at the crystal output. The initial pulse has Gaussian shape, and the parameters are  $T = 5$  ps,  $I = 5$  GW/cm<sup>2</sup>,  $\lambda_{in} = 532$  nm,  $\lambda_0 = 2\pi c/\omega_0 = 700$  nm, and  $d_{33} = \chi_{LT}^{(2)}/2 = 14$  pm/V.

generation is achieved by chirping the QPM grating. In this way, different processes can be matched in different points of the crystal. Chirped crystals have been exploited to implement broadband incoherent light sources for optical coherence tomography [28] or to generate entangled photons (biphotons) needed for nonclassical applications [9], [10]. We take the spatial frequency of the QPM crystal to be  $K(z) = K_0 - \zeta z$ , where  $K_0$  is chosen to phase-match a selected frequency at the beginning of the crystal, and  $\zeta$  is chosen to phase match a selected frequency at its output end. Being that  $K(z)$  is the instantaneous spatial frequency of the grating, the grating can be expanded as  $G(z) = \sum a_m \exp[i m \int_0^z K(s) ds]$  with being  $a_m = (2/\pi) \sin(m(\pi/2))$  the Fourier coefficient of a square wave. The power spectral density of the downconverted light (signal or idler) is governed by the phase-matching condition in the nonlinear structure that, in the low conversion limit, is given by

$$S(\omega_s) \propto \left| \int_0^L G(z) \exp[-i \Delta k(\omega_s) z] dz \right|^2. \quad (20)$$

We considered a periodically poled stoichiometric Lithium Tantalate sample (PPSLT) that is  $L = 2$  cm long, with initial local period  $T_0 = 2\pi/K_0 = 7.5$   $\mu\text{m}$  and chirp parameter  $\zeta = 6.24 \cdot 10^6$   $\text{m}^{-1}$ , that corresponds to a final local period  $T_L = 8.128$   $\mu\text{m}$ . This crystal has been exploited to implement a broadband light source for optical coherence tomography [28]. From (20), by modeling the refractive index dispersion with a Sellmeier equation [29] and assuming a temperature  $T = 80$  °C, we find that the band of parametric ranges from 800 to 1600 nanometers [see Fig. 2(a)]. By looking at the local first-order quasi phase matching curves in Fig. 2(b), we see that in the first part of the crystal, the parametric process is not phase matched. At around  $z = 7$  mm, the grating matches the process  $\omega_p \rightarrow \omega_p/2 + \omega_p/2$  and by increasing the propagation distance, the down converted photon pairs (signal and idler) are generated almost symmetrically around half the pump frequency, their separation increasing with propagation distance.

We simulated the propagation of a  $T = 5$  ps FWHM long Gaussian pulse, centered around 532 nm, with  $I = 5$  GW/cm<sup>2</sup> peak intensity. In the simulation, we set the reference wavelength  $\lambda_0 = 700$  nm. We assumed a nonlinear coefficient  $d_{33} = \chi_{LT}^{(2)}/2 = 14$  pm/V and modeled the square-wave QPM grating as a sum of spatial harmonics up to the fifth order. In the numerical code, we inserted the exact dispersion relation  $k(\omega)$  as obtained from Sellmeier relation; results of the simulation are shown in Fig. 2(c).

As expected from the analysis performed above, in the first 5 mm of propagation, nothing happens, since the spontaneous parametric down conversion process is not phase matched. Around  $z = 7$  mm, some energy is transferred from the pump to the idler/signal at half the pump frequency. During the propagation, a uniform broadening of the down converted light takes place to the output face of the crystal, where a uniform plateau of spectral intensity ranges from 800 to

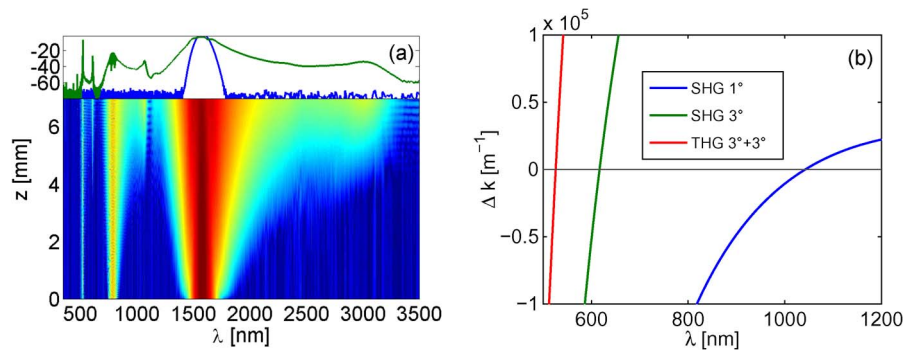


Fig. 3. (a) Evolution of the power spectrum (in decibels) from numerical solution of (18) and power spectrum profile at the crystal output. The initial pulse has Gaussian shape, and the parameters are  $T = 50$  fs,  $I = 11$  GW/cm<sup>2</sup>,  $\lambda_{in} = 1580$  nm,  $\lambda_0 = 2\pi c/\omega_0 = 700$  nm, and  $d_{33} = \chi_{LN}^{(2)}/2 = 27$  pm/V. (b) Phase-matching curves for the second harmonic generation (I and III order) and direct third harmonic generation (III order).

1600 nm. In this case, the conversion efficiency is lower than in the previous case, because the different frequency bands are phase matched only in portions of the crystal, rather than for the entire length, as before. The fact that the first part of the grating matches no any process suggests that a smarter design of the chirped grating would allow an increment of the conversion efficiency.

### 3.3. Spectral Broadening and Harmonic Generation of Femtosecond Pulses

As a last example, we consider the propagation of a femtosecond pulse into a highly mismatched periodically poled LN (PPLN) sample that was demonstrated experimentally to generate an octave spanning supercontinuum spectral broadening [3]. We assumed a QPM grating with a period  $\Lambda = 30$   $\mu\text{m}$  (phase matched for second harmonic generation at around  $2$   $\mu\text{m}$  fundamental wavelength). As before, we included higher order QPM terms, since the huge bandwidth can phase match different spatial harmonics. We injected a  $T = 50$  fs FWHM long Gaussian pulse, centered around 1580 nm, with  $I = 11$  GW/cm<sup>2</sup> peak intensity. In the simulation, we set the reference wavelength  $\lambda_0 = 700$  nm. Fig. 3(a) shows the evolution of the spectrum during the propagation into a  $L = 7$  mm crystal. We can see a consistent broadening and redshift of the FF part of the spectrum that, at the end of the crystal, reaches an octave-spanning bandwidth from 1200 nm to 3000 nm. We can also see the generation of spectral component at the second and third harmonics. At the second harmonic, the spectrum initially broadens and has an evolution ruled by highly mismatched SHG. When the FF broadening reaches the first-order quasi phase matching wavelength at around  $2$   $\mu\text{m}$ , the more-efficient conversion process generates a spike at around  $1$   $\mu\text{m}$ .

At the crystal output, we can see a broadband second and third harmonic of the broadened laser spectrum, as well as the presence of some spikes given by the quasi phase matching of high order spatial harmonics of the grating. We verified [see Fig. 3(b)] that the two spikes at the third harmonic correspond to the third-order QPM SHG (614 nm) and to the direct third-harmonic generation (526 nm) [30]. We can also see a spectral overlap between the harmonics of the broadened laser spectrum that can be exploited to achieve carrier-envelope-offset phase slip stabilization [3] that is of paramount importance for frequency metrology applications.

The infrared part of the spectrum exhibits more than an octave spanning between 1300 nm and 3000 nm at the  $-40$ -dB spectral power lower with respect to the peak power level. The spectral components near the zero GVM wavelength around 3000 nm are generated more efficiently. This is due to a first-order phase-matched parametric process between a pump at  $\lambda = 1070$  nm that is down converted to  $\lambda = 1650$  nm and  $\lambda = 3017$  nm. All the features described above compare surprisingly well with the experimental results of Langrock *et al.* [3].

## 4. Conclusion

In conclusion, we presented a comprehensive framework to study the nonlinear evolution of ultrabroadband optical pulses in quadratic nonlinear media. We employed a nonlinear envelope equation that allows to treat all the harmonics by means of a single equation. We exploited this model to simulate recently observed supercontinuum phenomena such as ultrabroadband parametric down-conversion and the generation of octave-spanning spectra from femtosecond pulses.

## Appendix Conserved Quantities

### Field Intensity

First, we show that (5) has the following conserved quantity, proportional to the total intensity of the field:

$$I_E = \int |\hat{E}(\omega, z)|^2 n(\omega) d\omega \quad (21)$$

where the integration is intended from  $-\infty$  to  $+\infty$ , and  $n(\omega)$  is assumed to be real (lossless medium). We prove this property for a quadratic instantaneous nonlinear polarization  $\hat{P}_{NL}(z, \omega) = \varepsilon_0 \chi^{(2)} \mathcal{F}[E(z, t)^2](\omega) = \varepsilon_0 \chi^{(2)} [\hat{E} \star \hat{E}](\omega)$  (symbol  $\star$  denotes convolution), but the proof can be easily extended to any order of instantaneous nonlinearity. We have

$$\begin{aligned} \frac{dI_E}{dz} &= \int n(\omega) \left[ \frac{\partial \hat{E}}{\partial z} \hat{E}^* + \frac{\partial \hat{E}^*}{\partial z} \hat{E} \right] d\omega \\ &= -i \frac{\chi^{(2)}}{2c} \left[ \iint \omega \hat{E}(\omega') \hat{E}(\omega - \omega') \hat{E}^*(\omega) d\omega d\omega' - \iint \omega \hat{E}^*(\omega') \hat{E}^*(\omega - \omega') \hat{E}(\omega) d\omega d\omega' \right] \\ &= -i \frac{\chi^{(2)}}{2c} [J_1 - J_2]. \end{aligned}$$

By exploiting the Hermiticity of  $\hat{E}$  and by the change of variables ( $\omega \rightarrow -\omega, \omega' \rightarrow -\omega'$ ) in the integral  $J_1$ , we obtain  $J_1 = -J_2$  so that

$$\begin{aligned} \frac{dI_E}{dz} &= -2i \frac{\chi^{(2)}}{2c} \iint \omega \hat{E}(\omega') \hat{E}(\omega - \omega') \hat{E}^*(\omega) d\omega d\omega' \\ &= \frac{\chi^{(2)}}{c} \int [i\omega \hat{E}(\omega)]^* \left[ \int \hat{E}(\omega') \hat{E}(\omega - \omega') d\omega' \right] d\omega \\ &= \frac{\chi^{(2)}}{c} \int [i\omega \hat{E}(\omega)]^* [\hat{E} \star \hat{E}](\omega) d\omega. \end{aligned}$$

By exploiting Parseval's theorem (i.e., conservation of scalar product), we can write the integral in the time domain, and considering that the field must vanish at infinity, we have

$$\frac{dI_E}{dz} = \frac{\chi^{(2)}}{c} \int \frac{\partial E(t)}{\partial t} E(t)^2 dt = \frac{\chi^{(2)}}{3c} E(t)^3 \Big|_{-\infty}^{+\infty} = 0.$$

### Envelope Intensity

Now, we consider NEE (14) with the exact nonlinear second-order polarization (17) (the change of reference frame travelling at the group velocity obviously does not affect the energy conservation)

$$\frac{\partial A}{\partial z} + iD'A = -i\sigma \left( 1 - \frac{i}{\omega_0} \frac{\partial}{\partial t} \right) \left[ A^2 e^{i\alpha} + \left( |A|^2 + \frac{i}{\pi t} \star |A|^2 \right) e^{-i\alpha} \right] \quad (22)$$

where  $\sigma = (\omega_0 \chi^{(2)}) / (4n_0 c)$ ,  $\alpha = \omega_0 t - \beta_0 z$ . In this case, since, in its derivation, we assumed  $n(\omega) \approx n(\omega_0)$  in front of the nonlinear term, the conserved quantity reduces to

$$I_A = \int |\hat{A}(\omega, z)|^2 d\omega = \int |A(t, z)|^2 dt. \quad (23)$$

We have

$$\frac{dI_A}{dz} = \sigma \int \left\{ -i|A|^2 A e^{i\alpha} - i|A|^2 A^* e^{-i\alpha} + A^* \frac{1}{\pi t} \star |A|^2 e^{-i\alpha} - \frac{1}{\omega_0} A^* \frac{\partial}{\partial t} \left[ A^2 e^{i\alpha} + |A|^2 e^{-i\alpha} + \frac{i}{\pi t} \star |A|^2 e^{-i\alpha} \right] \right\} dt + c.c.$$

After two integration by parts and some algebra, we obtain

$$\frac{dI_A}{dz} = \frac{\sigma}{\omega_0} \int \left\{ A \frac{\partial |A|^2}{\partial t} + iA \frac{\partial}{\partial t} \left[ \frac{1}{\pi t} \star |A|^2 \right] \right\} e^{i\alpha} dt + c.c. = \frac{\sigma}{\omega_0} \int A e^{i\alpha} \left[ \frac{\partial |A|^2}{\partial t} - \frac{i}{\pi t} \star \frac{\partial |A|^2}{\partial t} \right]^* dt + c.c.$$

Again, we exploit the Parseval theorem and rewrite the scalar product in the frequency domain:

$$\frac{dI_A}{dz} = \frac{\sigma}{\omega_0} \int \hat{A}(\omega - \omega_0) e^{-i\beta_0 z} \left( \mathcal{F} \left[ \frac{\partial |A|^2}{\partial t} \right] (\omega) 2H(-\omega) \right)^* d\omega + c.c.$$

where  $H(\omega)$  is Heaviside step function. This last integral vanishes because it is the product of two functions with non-overlapping supports. In fact,  $\text{supp}\{\hat{A}(\omega - \omega_0)\} = (0, +\infty)$  by definition of the envelope, and  $\text{supp}\{H(-\omega)\} = (-\infty, 0)$ .

It is possible to demonstrate that (18) also conserves the quantity  $I_A$ . In this case, the proof can be performed straightforwardly in the time domain by successive integration by parts.

## References

- [1] J. M. Dudley, G. Genty, and S. Coen, "Supercontinuum generation in photonic crystal fiber," *Rev. Mod. Phys.*, vol. 78, no. 4, pp. 1135–1184, Oct.–Dec. 2006.
- [2] R. W. Boyd, *Nonlinear Optics*, 2nd ed. New York: Academic, 2003.
- [3] C. Langrock, M. M. Fejer, I. Hartl, and M. E. Fermann, "Generation of octave-spanning spectra inside reverse-photon-exchanged periodically poled lithium niobate waveguides," *Opt. Lett.*, vol. 32, no. 17, pp. 2478–2480, Sep. 2007.
- [4] O. Prakash, H.-H. Lim, B.-J. Kim, K. Pandiyan, M. Cha, and B. K. Rhee, "Collinear broadband optical parametric generation in periodically poled lithium niobate crystals by group velocity matching," *Appl. Phys. B, Photophys. Laser Chem.*, vol. 92, no. 4, pp. 535–541, Sep. 2008.
- [5] M. Tiihonen, A. Pasiskevicius, V. Fragemann, C. Canalias, and F. Laurell, "Ultrabroad gain in an optical parametric generator with periodically poled KTiOPO<sub>4</sub>," *Appl. Phys. B, Photophys. Laser Chem.*, vol. 85, no. 1, pp. 73–77, Oct. 2006.
- [6] R. S. S. Kumar, S. S. Harsha, and S. N. Nao, "Broadband supercontinuum generation in a single potassium dihydrogen phosphate (KDP) crystal achieved in tandem with sum frequency generation," *Appl. Phys. B, Photophys. Laser Chem.*, vol. 86, no. 4, pp. 615–621, Mar. 2007.
- [7] N. K. M. N. Srinivas, S. S. Harsha, and D. N. Rao, "Femtosecond supercontinuum generation in a quadratic nonlinear medium (KDP)," *Opt. Express*, vol. 13, no. 9, pp. 3224–3229, May 2005.
- [8] M. Conforti, F. Baronio, and C. De Angelis, "From femtosecond infrared to picosecond visible pulses: Temporal shaping with high-efficiency conversion," *Opt. Lett.*, vol. 32, no. 13, pp. 1779–1781, Jul. 2007.
- [9] S. E. Harris, "Chirp and compress: Toward single-cycle biphotons," *Phys. Rev. Lett.*, vol. 98, no. 6, p. 063602, Feb. 2007.
- [10] M. B. Nasr, S. Carrasco, B. E. Saleh, A. V. Segienko, M. C. Teich, J. P. Torres, L. Torner, D. Hum, and M. Fejer, "Ultrabroadband biphotons generated via quasi-phase-matched optical parametric down-conversion," *Phys. Rev. Lett.*, vol. 100, no. 18, p. 183 601, May 2008.
- [11] A. F. Abouraddy, M. B. Nasr, B. E. A. Saleh, A. V. Sergienko, and M. C. Teich, "Quantum-optical coherence tomography with dispersion cancellation," *Phys. Rev. A, Gen. Phys.*, vol. 65, no. 5, p. 053817, May 2002.
- [12] M. Marangoni, D. Bida, M. Conforti, A. D. Capobianco, C. Manzoni, F. Baronio, G. F. Nalesso, C. De Angelis, R. Ramponi, and G. Cerullo, "Synthesis of picosecond pulses by spectral compression and shaping of femtosecond pulses in engineered quadratic nonlinear media," *Opt. Lett.*, vol. 34, no. 3, pp. 241–243, Feb. 2009.
- [13] T. Brabec and F. Krausz, "Nonlinear optical pulse propagation in the single-cycle regime," *Phys. Rev. Lett.*, vol. 78, no. 17, pp. 3282–3285, Apr. 1997.

- [14] M. Geissler, G. Tempea, A. Scrinzi, M. Schnurer, F. Krausz, and T. Brabec, "Light propagation in field-ionizing media: Extreme nonlinear optics," *Phys. Rev. Lett.*, vol. 83, no. 15, pp. 2930–2933, Oct. 1999.
- [15] T. Brabec and F. Krausz, "Intense few-cycle laser fields: Frontiers of nonlinear optics," *Rev. Mod. Phys.*, vol. 72, no. 2, pp. 545–591, Apr. 2000.
- [16] A. V. Housakou and J. Herrmann, "Supercontinuum generation of higher-order solitons by fission in photonic crystal fibers," *Phys. Rev. Lett.*, vol. 87, no. 20, p. 203901, Nov. 2001.
- [17] M. Kolesik, J. V. Moloney, and M. Mlejnek, "Unidirectional optical pulse propagation equation," *Phys. Rev. Lett.*, vol. 89, no. 28, p. 283902, Dec. 2002.
- [18] M. Kolesik and J. V. Moloney, "Nonlinear optical pulse propagation simulation: From Maxwell's to unidirectional equations," *Phys. Rev. E, Stat. Phys. Plasmas Fluids Relat. Interdiscip. Top.*, vol. 70, no. 11, p. 036604, Nov. 2004.
- [19] G. Genty, P. Kinsler, B. Kibler, and J. M. Dudley, "Nonlinear envelope equation modeling of sub-cycle dynamics and harmonic generation in nonlinear waveguides," *Opt. Express*, vol. 15, no. 9, pp. 5382–5387, Apr. 2007.
- [20] P. Kinsler and G. H. C. New, "Few-cycle pulse propagation," *Phys. Rev. A, Gen. Phys.*, vol. 67, no. 2, p. 023813, Feb. 2003.
- [21] P. Kinsler, S. B. P. Radnor, and G. H. C. New, "Theory of directional pulse propagation," *Phys. Rev. A, Gen. Phys.*, vol. 72, no. 11, p. 063807, Nov. 2005.
- [22] P. Kinsler, "Optical pulse propagation with minimal approximations," *Phys. Rev. A, Gen. Phys.*, vol. 81, no. 1, p. 013819, Jan. 2010.
- [23] A. Kumar, "Ultrashort pulse propagation in a cubic medium including the Raman effect," *Phys. Rev. A, Gen. Phys.*, vol. 81, no. 1, p. 013807, Jan. 2010.
- [24] M. Conforti, F. Baronio, and C. De Angelis, "Nonlinear envelope equation for broadband optical pulses in quadratic media," *Phys. Rev. A, Gen. Phys.*, vol. 81, no. 5, p. 053841, May 2010.
- [25] S. Haykin, *Communication System*, 4th ed. New York: Wiley, 2001.
- [26] D. H. Jundt, "Temperature-dependent Sellmeier equation for the index of refraction,  $n_e$ , in congruent lithium niobate," *Opt. Lett.*, vol. 22, no. 20, pp. 1553–1555, Oct. 1997.
- [27] P. S. Kuo, K. L. Vodopyanov, M. M. Fejer, D. M. Simanovskii, X. Yu, J. S. Harris, D. Bliss, and D. Weyburne, "Optical parametric generation of a mid-infrared continuum in orientation-patterned GaAs," *Opt. Lett.*, vol. 31, no. 1, pp. 71–73, Jan. 2006.
- [28] N. Mohan, O. Minaeva, G. N. Goltsman, M. F. Saleh, M. B. Nasr, A. V. Sergienko, B. E. Saleh, and M. C. Teich, "Ultrabroadband coherence-domain imaging using parametric downconversion and superconducting single-photon detectors at 1064 nm," *Appl. Opt.*, vol. 40, no. 20, pp. 4009–4017, Jul. 2009.
- [29] A. Bruner, D. Eger, M. B. Oron, P. Blau, and M. Katz, "Temperature-dependent Sellmeier equation for the refractive index of stoichiometric lithium tantalate," *Opt. Lett.*, vol. 28, no. 3, pp. 194–196, Feb. 2003.
- [30] S. K. Das, S. Mukhopadhyay, N. Sinha, A. Saha, P. K. Datta, S. M. Saitiel, and L. C. Andreani, "Direct third harmonic generation due to quadratic cascaded processes in periodically poled crystals," *Opt. Commun.*, vol. 262, no. 1, pp. 108–113, Jan. 2006.